

Dariusz GRZESIAK^{a,*}, Bandar ALMANGOUR^b, Paweł FIGIEL^a, Sebastian FRYSKA^a

^a Faculty of Mechanical Engineering and Mechatronics, West Pomeranian University of Technology Szczecin, Poland


^b Saudi Arabia Basic Industries Corporation, Jubail, Saudi Arabia

* Corresponding author: dariusz.grzesiak@zut.edu.pl

SELECTIVE LASER MELTING OF H13-TiB₂ METAL MATRIX COMPOSITES – THE ROLE OF VOLUMETRIC ENERGY DENSITY

© 2019 Dariusz Grzesiak, Bandar AlMangour, Paweł Figiel, Sebastian Fryska

This is an open access article licensed under the Creative Commons Attribution International License (CC BY)

 <https://creativecommons.org/licenses/by/4.0/>

Key words: H13 tool steel, TiB₂, SLM, Selective Laser Melting, volumetric energy density.

Abstract: The paper presents an analysis of the impact of the volumetric energy density delivered during the Selective Laser Melting (SLM) of a mixture of H13 tool steel powder and microcrystalline TiB₂, on the properties of the obtained metallic matrix composite. The results of measurements of density and hardness as well as microscopic analysis of six variants of the obtained composite, differing in the value of energy density provided by the laser beam and the number of passes of this beam on each fused layer, are presented. The results show that, in the case of a metallic matrix composite, the increase in the volumetric energy density supplied during the SLM process can lead to the deterioration of the material properties.

Selektywne stapanie laserowe kompozytu w osnowie metalicznej H13-TiB₂ – wpływ objętościowej gęstości energii

Słowa kluczowe: stal narzędziowa H13, TiB₂, SLM, selektywne stapanie laserowe, objętościowa gęstość energii.

Streszczenie: Artykuł przedstawia analizę wpływu objętościowej gęstości energii dostarczanej podczas selektywnego stapania laserowego mieszaniny proszku stali H13 oraz mikrokrystalicznego TiB₂ na właściwości uzyskanego w ten sposób kompozytu w osnowie metalicznej. Przedstawiono wyniki pomiarów gęstości i twardości oraz analizę mikroskopową sześciu wariantów otrzymanego kompozytu, różniących się wartością gęstości energii dostarczanej przez wiązkę lasera i ilością przejść tej wiązki na każdej stapianej warstwie. Wyniki pokazują, że w przypadku kompozytu w osnowie metalicznej zwiększanie objętościowej gęstości energii dostarczanej przy stapaniu może prowadzić do pogorszenia właściwości materiału.

Introduction

Type H13 steel is a medium-carbon, hot work steel, which can be subjected to extremely high loads that are applied rapidly and under high-temperature gradients [1]. It exhibits high elastic strength, wear resistance, and high-temperature stability [2, 3]. One way to improve the properties of such hard-working materials is by incorporating hard second-phase reinforcement into the steel matrix. Such particulate-reinforced metal matrix composites (MMCs) have received considerable attention because of their improved wear resistance, reduced cost, isotropic properties, and low density [4, 5].

A specific way to produce fine-structured MMC materials is the use of mechanical alloying in combination with laser-based additive manufacturing (in this specific case, Selective Laser Melting – SLM). Mechanical alloying is a non-equilibrium, low-temperature, and solid-state powder processing technique [6, 7]. The process involves the repeated deformation, fracturing, and cold welding of powder particles in a high-energy ball mill. SLM is a powder bed additive manufacturing technology in which the energy provided by the laser beam melts the metal powder particles in a layer-by-layer manner. The rapid solidification rate occurring in the SLM process eliminates phase segregation (i.e. promotes better chemical homogeneity) and produces

a very fine microstructure with a uniform size distribution of non-metallic inclusions [8, 9]. SLM technology is currently widely used in unit and small lot production of metallic parts, the processing of hardly workable alloys, bioengineering metal matrix composites, metallic glasses fabrication, and many others [10, 11, 12].

1. Raw material preparation

The powder used in this study was the mixture of a spherical gas atomized AISI H13 steel powder with an average particle size of $\sim 45\mu\text{m}$ (Fig. 2A) and a TiB_2 powder with an average particle size $2\text{--}12\mu\text{m}$ (Fig. 2B). Before mixing with TiB_2 , the H13 powder was sieved using an LPzE-2e (MULTISERW-Morek) laboratory shaker equipped with a $53\mu\text{m}$ sieve. The mechanical alloying process was carried out in a high-energy ball mill (Pulverisette 6, Fritsch GmbH) using a 5:1 ball-to-powder ratio and 200 rpm speed for a period of 8 h. The milling process was conducted in an argon protective atmosphere. In order to avoid an excessive temperature rise within the grinding bowl, there was a 15-min pause after each 1 h milling cycle. The volume ratio of the components was 85% (H13) to 15% (TiB_2), which was the result of a previously conducted research [11–14].

2. SLM process

The feedstock powder obtained by the mechanical alloying process was used to fabricate cylindrical samples with a diameter of 10mm and a height of 6mm. Two different scanning strategies and three different sets of process parameters were used, resulting in six different sample fabrication conditions (Tab. 1). Different process parameters were aimed to achieve different volumetric energy density [15] (E_{density}) supplied to the processed material. E_{density} represents the energy supplied by the laser beam to a volumetric unit of the powder, and it is equal to the laser power (P) divided by the result of multiplication of a scanning speed (V), hatching space

(h), and layer thickness (d). In turn, the scanning speed represents the ratio of the distance between every melted spot (a) to the exposition time of the laser beam in it (t). The exact meaning of the above parameters is shown in Figure 1A. Figures 1B and C shows the scanning strategies used in this study, which is described as an “alternate hatches” pattern, in which a layer is scanned by a laser beam once or twice and then a 90deg rotation of hatches is applied on the next layer. All samples were manufactured on a steel base plate preheated to 200C degrees. The SLM process was conducted in an argon protective atmosphere with an oxygen level below 0.5%.

Table 1. Summary of processing parameters used in the experiment

No.	E_{density} [J/mm ³]	V [mm/s]	P [W]	h [mm]	D [mm]	a [mm]	t [s]	Number of laser passes
1	60	278	100	0.12	0.05	0.08	0.000288	1
2	60	278	100	0.12	0.05	0.08	0.000288	2
3	80	208	100	0.12	0.05	0.08	0.000384	1
4	80	208	100	0.12	0.05	0.08	0.000384	2
5	100	167	100	0.12	0.05	0.08	0.00048	1
6	100	167	100	0.12	0.05	0.08	0.00048	2

3. Material characterizations

The microstructures of the fabricated composites were analysed using a HITACHI SU scanning electron microscope equipped with a THERMO FISHER NORAN 7 microanalysis adapter and a FEI Nova Nano 230 scanning electron microscope. Specimens for metallographic examinations were prepared according to the standard metallographic procedures. The relative densities of each composite variant were calculated based on the Archimedes principle. The Vickers hardness values of the SLM-fabricated composites were measured using a LECO LM247AT microhardness tester with a load of 0.03 kG and an indentation time of 10 s.

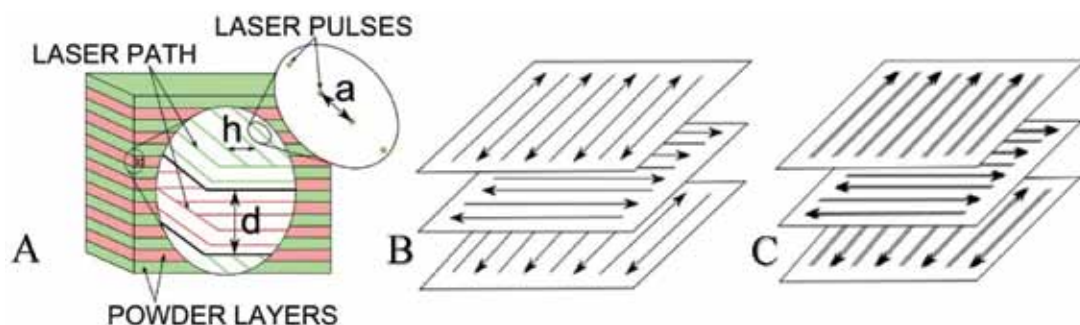


Fig. 1. The meaning of process parameters (A) and scanning strategies applied in the study: B – alternate hatches, single pass of the laser beam; C – alternate hatches, double pass of the laser beam

Source: Authors.

3. Results and discussion

After 8 h of milling, some of the milled $\text{TiB}_2/\text{H13}$ steel particles retained their spherical morphology, while some were flattened, as shown in Fig. 2C. A spherical morphology suggests the effectiveness of the milling procedure for SLM.

The density measurements results (Fig. 3) revealed that there is a clearly visible downward trend related to increasing volumetric energy density in both once and twice scanned samples. Particularly noteworthy is the fact that double laser scanning caused a significant decrease in density in all cases of the energy density

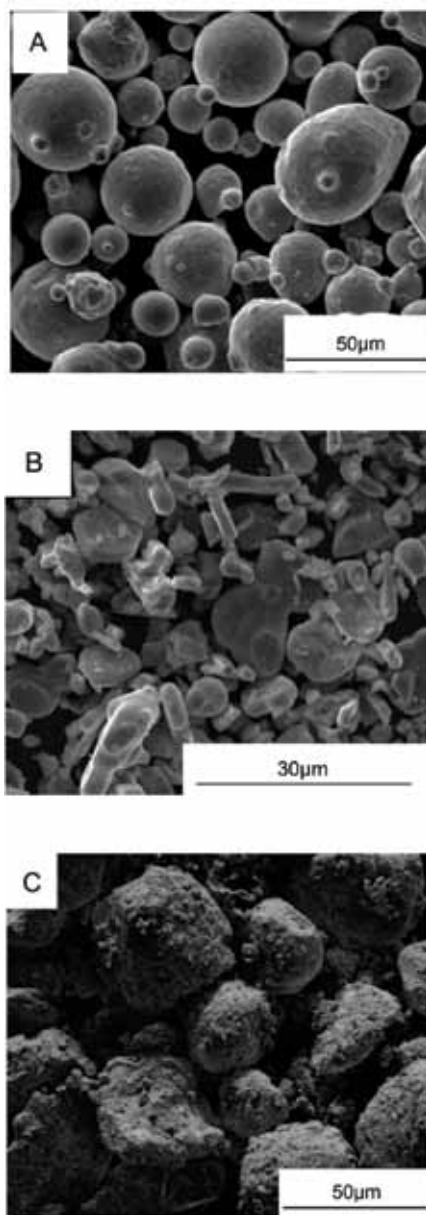


Fig. 2. SEM images of the starting materials: A – H13 tool steel powder, B – TiB_2 powder, C – H13/ TiB_2 mixture after ball milling

Source: Authors.

analysed. This phenomenon is opposite to the typical increase in the density of metallic materials processed using SLM technology, which occurs with increasing density of energy supplied [16, 17]. It follows that its origin should be sought in the application of TiB_2 as a reinforcing phase. The probable explanation may be the high viscosity of the molten metal, which causes its attraction to the particles of the strengthening phase, thereby disrupting the uniform distribution of the material on each layer. As shown in the microscopic studies in the further part of the article, the particles of the strengthening phase showed a tendency to form agglomerates, which increases with the increase of energy density, which may also enhance the above phenomenon. As a consequence, this led to an uneven thickness of each subsequent layer of powder applied, and thus to the appearance of places where the powder may not have been completely melted, and the additional liquefaction caused by the re-passage of the laser beam that has deepened this effect.

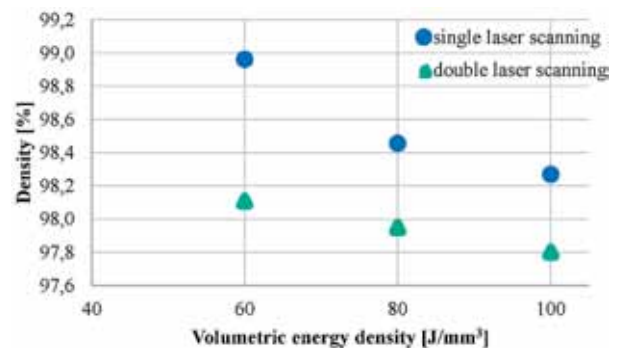


Fig. 3. Density measurements results

Source: Authors.

As showed in Figure 4, opposite trends in hardness values can be observed: In the case of the composite obtained by single laser scanning, there is a hardness decrease together with an increase of the energy density; whereas, in the case of the second material variant, the hardness increases. However, the values obtained for a double scanned material are noticeably lower until the 100 J/mm³ energy density is used, which is when the lowest value of a single scanned composite is reached. This interesting phenomenon may be explained by the lower density of the second variant of the composite, while the increasing hardness trend, which is contrary to the downward trend observed in the case of single scanned composites, may result from additional hardening of H13 steel, which is the result of an additional, short-term transition to the liquid state and back to the solid state, which facilitates the formation of new martensite nuclei. However, there is further crystallographic analysis required for an exact explanation.

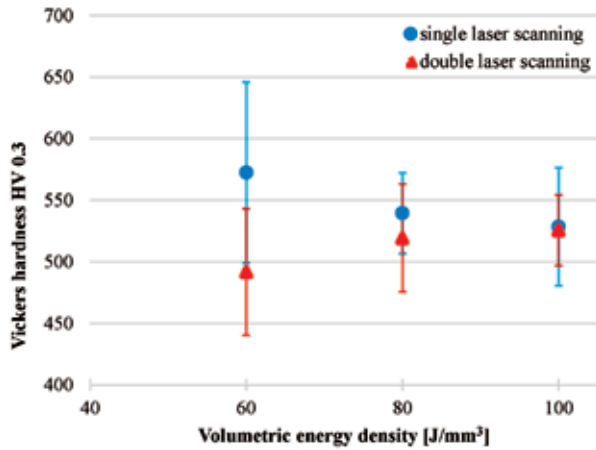


Fig. 4. Hardness measurements results

Source: Authors.

Figure 5 presents images obtained by a single laser scanning on each layer, and Figure 6 presents their double scanned counterparts. The X-ray diffraction of the composite, previously published by the authors [11], clearly confirmed the presence of the TiB_2 phase, both in

the powder mixture, and in the material obtained after the SLM process. The identification of this phase was performed on the basis of elemental mapping (in this case, Ti was chosen due to the fact that the boron lies at the limit of the traceability range in the EDS analysis), and it is shown in Figures 5 and 6 in the middle column. Figure 5A shows the composite manufactured using $60 J/mm^3$ energy density – the lower magnification image (left side) reveals good dispersion and uniform size of the reinforcing phase particles. Magnification of a single TiB_2 particle (right side) shows its correct integration into the matrix, and small cracks of the particle are also visible. Figure 5B shows the composite manufactured using $80 J/mm^3$ energy density, where a tendency to form agglomerates by the particles of the strengthening phase is noticeable, and the shapes of the particles become more extended. With the magnification of a single TiB_2 particle, cracks can also be observed. The third variant of a composite, which was manufactured using $100 J/mm^3$ energy density, is presented in Fig. 5C. A noticeable increase in the porosity of the structure is visible, as well as the tendency to form agglomerates,

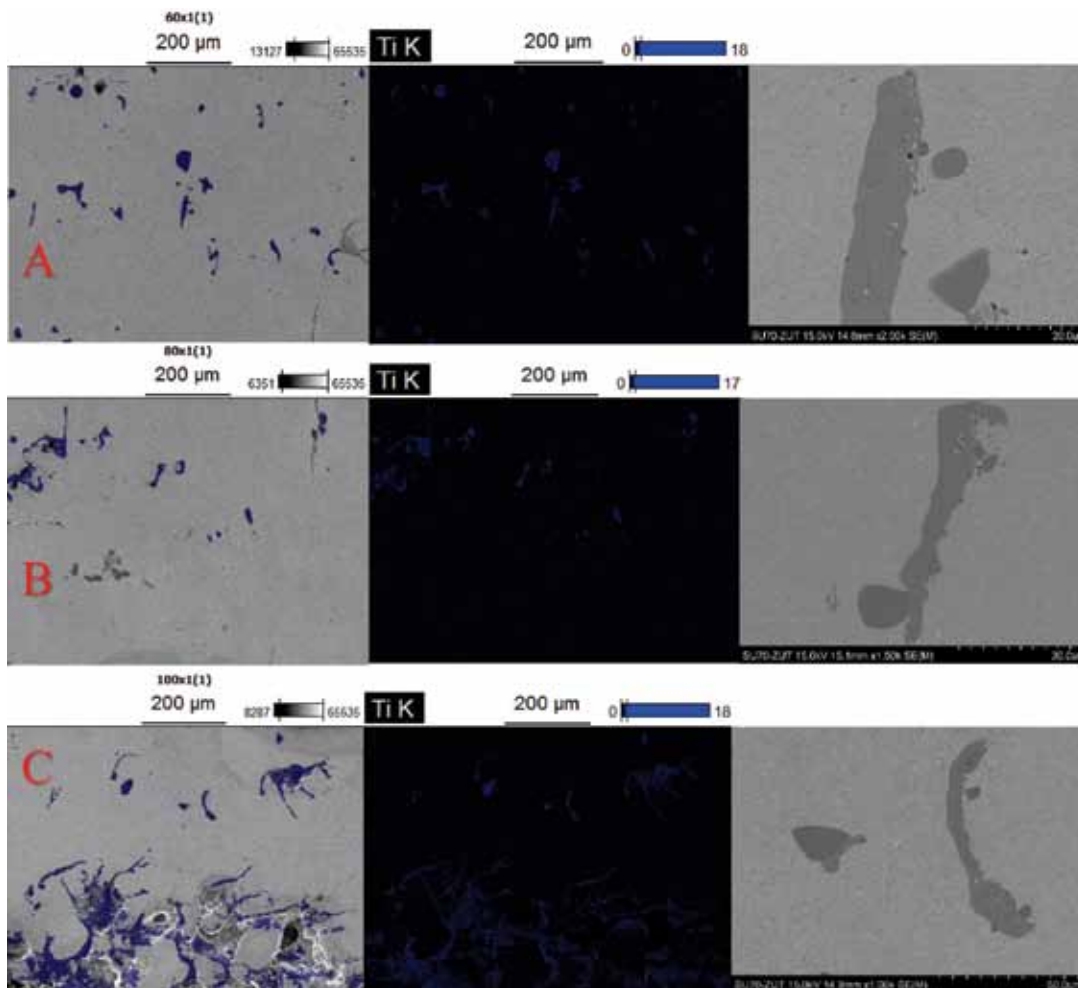


Fig. 5. SEM images of a single scanned composites: A – $60 J/mm^3$, B – $80 J/mm^3$, C – $100 J/mm^3$

Source: Authors.

which is even more advanced than in the 80 J/mm^3 composite. Worth noting is the fact that most of the reinforcing phase particles surround the pores and their shape is longitudinal. The cracks on the magnified particle can also be observed.

Figure 6A shows the composite obtained by use of 60 J/mm^3 and double laser scanning. In comparison to the structure shown in Figure 5A, the distribution of the strengthening phase particles has changed very clearly; they form agglomerates of elongated shape, similar to the results of higher energy densities used in the one-time scanned composites. Variants of the composite formed by double scanning of the laser providing either 80 J/mm^3 or 100 J/mm^3 are also characterized by a more noticeable agglomeration of the particles, and there is also noticeable porosity. Magnifications of individual particles, as before, show their small cracks.

SEM imaging showed a strong dependence of the structure of presented composites on the amount of energy supplied by the laser beam. Increasing the energy density and using additional laser scanning caused the

TiB_2 particles to concentrate into larger clusters and a tendency to form longitudinal fields. These phenomena may result from the dynamics of liquefied metal during the melting process, because the laser beam is pulsed rather than firing continuously, so the melted path consists of individual melted fields. Too much energy supplied by the laser in a single spot caused the scattering of the particles of the strengthening phase and set them in external areas. This was previously explained by Simchi and Asgharzadeh [18] and Gu et al. [19], who reported that Marangoni convection within the molten pool, generated by high temperature and high surface tension, induced a liquid capillary force that caused the rearrangement of reinforcing particles.

Conclusion

The presented research uses the method of changing the volume energy density by changing the exposure time of a laser beam in a single spot. This is

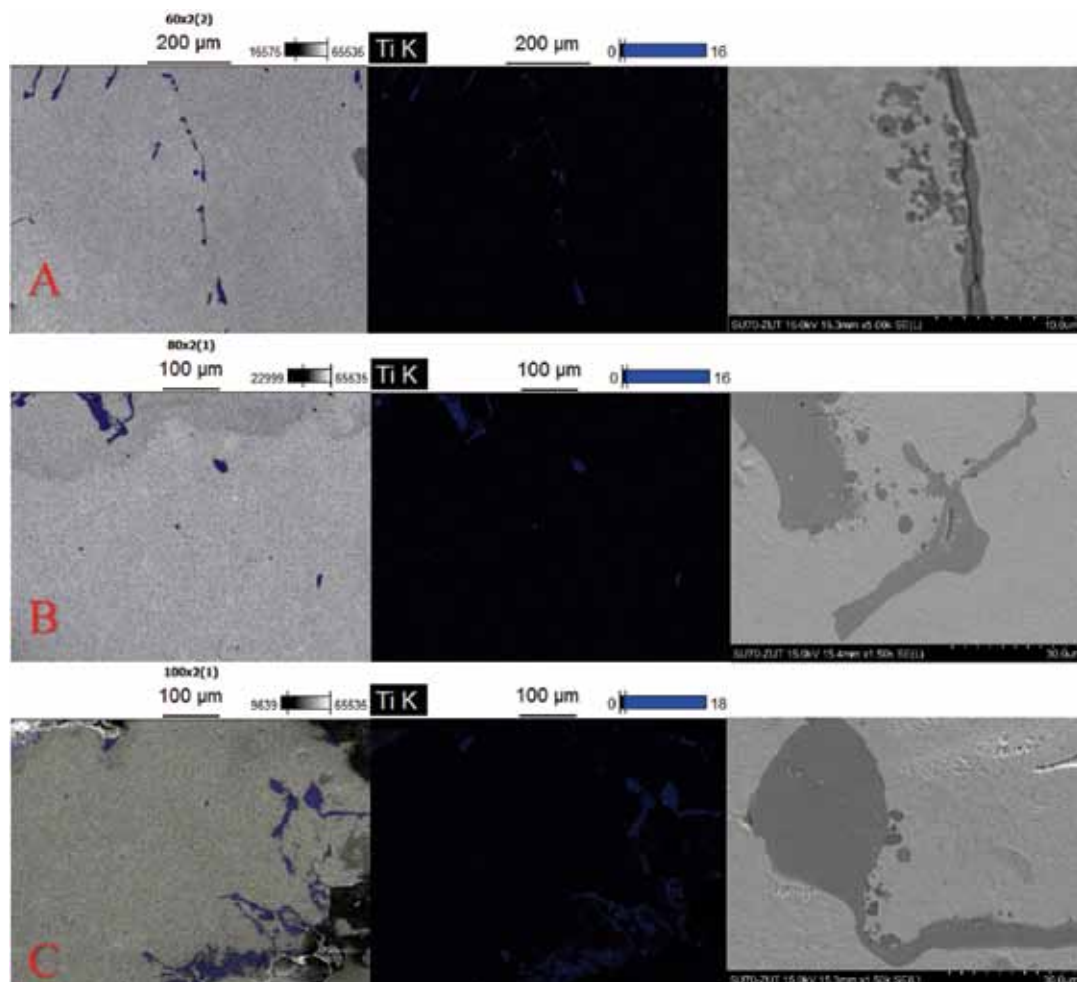


Fig. 6. SEM images of a double scanned composites: A – 60 J/mm^3 , B – 80 J/mm^3 , C – 100 J/mm^3
Source: Authors.

just one of the possibilities, because the same effect can be theoretically obtained by changing the laser power, the thickness of the layer, the distance between the laser tracks, or the distance between individual melted spots. Recent scientific work in this field [20] indicates that this approach can give completely different results; therefore, it is a reasonable direction for further research.

References

1. Shackelford J.F., Han Y.H., Kim S., Kwon S.H.: *CRC Materials Science and Engineering Handbook*. Boca Raton: CRC Press, 2015.
2. Krauss G.: *Steels: Processing, Structure, and Performance*. Materials Park: ASM International, 2015.
3. Hashmi S.: *Comprehensive Materials Processing*. Elsevier, 2014.
4. Ibrahim I., Mohamed F., Lavernia E.: Particulate reinforced metal matrix composites — a review. *Journal of Materials Science*, 1991, 26, pp. 1137–1156.
5. Tjong S.C.: Novel nanoparticle-reinforced metal matrix composites with enhanced mechanical properties. *Advanced Engineering Materials*, 2007, 9, pp. 639–652.
6. Akhtar F.: Microstructure evolution and wear properties of in situ synthesized TiB₂ and TiC reinforced steel matrix composites. *Journal of Alloys and Compounds*, 2008, 459, pp. 491–497.
7. Jiang W., Molian P.: Nanocrystalline TiC powder alloying and glazing of H13 steel using a CO₂ laser for improved life of die-casting dies. *Surface and Coatings Technology*, 2001, 135, pp. 139–149.
8. Kruth J.P., Mercelis P., Van Vaerenbergh J., Froyen L., Rombouts M.: Binding mechanisms in selective laser sintering and selective laser melting. *Rapid Prototyping Journal*, 2005, 11, pp. 26–36.
9. Rombouts M., Kruth J.P., Froyen L., Mercelis P.: Fundamentals of selective laser melting of alloyed steel powders. *CIRP Annals – Manufacturing Technology*, 2006, 55, pp. 187–192.
10. Uklejewski R., Winiecki M., Rogala P., Mielniczuk J.: Selective laser melted prototype of original minimally invasive resurfacing hip endoprosthesis. *Rapid Prototyping Journal*, 2011, 17, pp. 76–85.
11. AlMangour B., Grzesiak D., Yang J.M.: Selective laser melting of TiB₂/H13 steel nanocomposites: Influence of hot isostatic pressing post-treatment. *Journal of Materials Processing Technology*, 2017, 244, pp. 1–10.
12. AlMangour B., Yu F., Yang J.M., Grzesiak D.: Selective laser melting of TiC/H13 steel bulk-form nanocomposites with variations in processing parameters. *MRS Communications*, 2017, 7, pp. 84–89.
13. AlMangour B., Grzesiak D., Yang J.M.: Nanocrystalline TiC-reinforced H13 steel matrix nanocomposites fabricated by selective laser melting. *Materials and Design*, 2016, 96, pp. 150–161.
14. Deirmina F., AlMangour B., Grzesiak D., Pellizzari M.: H13–partially stabilized zirconia nanocomposites fabricated by high-energy mechanical milling and selective laser melting. *Materials and Design*, 2018, 146, pp. 286–297.
15. Vandenbroucke B., Kruth J.P.: Selective laser melting of biocompatible metals for rapid manufacturing of medical parts. *Rapid Prototyping Journal*, 2007, 13 (4), pp. 196–203.
16. Tucho W.M., Lysne V.H., Austbø H., Sjolyst-Kverneland A., Hansen V.: Investigation of effects of process parameters on microstructure and hardness of SLM manufactured SS316L. *Journal of Alloys and Compounds*, 2018, 740, pp. 910–925.
17. Zhang B., Bi G., Nai S., Sun Ch.N., Wei J.: Microhardness and microstructure evolution of TiB₂ reinforced Inconel 625/TiB₂ composite produced by selective laser melting. *Optics & Laser Technology*, 2016, 80, pp. 186–195.
18. Simchi A., Asgharzadeh H.: Densification and microstructural evaluation during laser sintering of M2 high speed steel powder. *Journal of Materials Science & Technology*, 2004, 20, pp. 1462–1468.
19. Gu D., Shen Y., Fang S., Xiao J.: Metallurgical mechanisms in direct laser sintering of Cu–CuSn–CuP mixed powder. *Journal of Alloys and Compounds*, 2007, 438, pp. 184–189.
20. Prashanth K.G., Scudino S., Maity T., Das J., Eckert J.: Is the energy density a reliable parameter for materials synthesis by selective laser melting? *Materials Research Letters*, 2017, 5, pp. 386–390.